Supplement of Atmos. Chem. Phys., 26, 9037–9060, 2026
https://doi.org/10.5194/acp-26-9037-2026-supplement

Atmospheric Chemistry and Physics
Open Access

Supplement of

Residential burning is a potentially significant source of soluble iron to the ocean

Rui Li et al.

Correspondence to: Douglas S. Hamilton (dshamil3@ncsu.edu) and Mingjin Tang (mingjintang@126.com)

S1 Experimental methods and results

S1.1 Experimental methods

Figure S1 show the schematic diagram of the apparatus used to generate and collect aerosol emitted by residential coal and biofuel combustion, and Figure S2 displays one of its photos taken during the sampling.

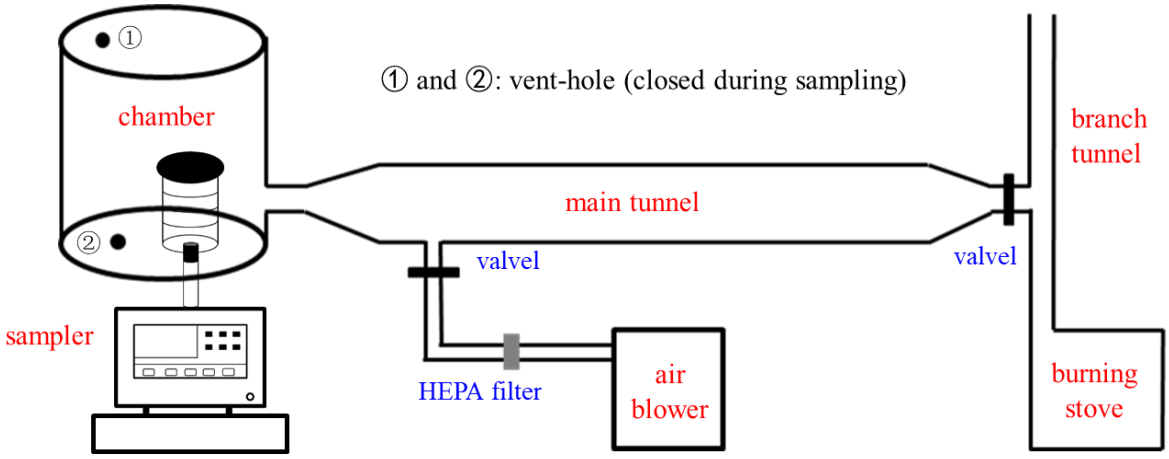

Figure S1. Schematic diagram of the apparatus used in our work to collect aerosol particles emitted by domestic coal and biofuel burning.

As shown in Figure 1, coal and biofuel were burned in a commercial cook stove, which is widely used in rural areas in China. Exhaust in the chimney, generated by coal and biofuel combustion, could go directly to the ambient air, or alternatively it could enter a horizontally-mounted long metal tube (inner diameter: 30 cm; length: 200 cm). After exiting the long metal tube, the exhaust entered a vertically-mounted chamber (inner diameter: 45 cm; height: 50 cm), and $PM_{2.5}$ was collected onto pre-cleaned Whatman 41 (W41) cellulose filters (diameter: 88 mm) via a medium volume aerosol sampler (TH-150C, Tianhong Co.) operated at a flow rate of 100 L/min. Filters were cleaned to reduce background using the procedure detailed elsewhere (Zhang et al., 2022). Aerosol sampling was stopped automatically when the pressure

dropped to the threshold because of accumulation of aerosol on the filter, and sampling times ranged from a few to tens of minutes, varying for fuel types. Between combustion experiments, the tube was flushed to remove smoke generated from the previous combustion experiment.

Figure S2. A photo of the apparatus used in our work to collect aerosol particles emitted by domestic coal and biofuel burning.

S1.2 Experimental results

S1.2.1 Fe content of municipal waste fly ash, oil fly ash and oil bottom ash

For the three municipal waste fly ash samples we investigated, Fe content ranged from 3.9 to 29.7 mg/g, with average and median values being 18.7 ± 13.3 and 22.6 mg/g (Table S5). Several previous studies measured Fe content in municipal waste fly ash (Table S6). For example, the average Fe content were measured to be 18.0 ± 13.3 mg/g (n = 3) and 23.1 mg/g (n = 1) in two studies (Cobo et al., 2009; Raclavská et al., 2017), very similar to our results; another four studies (Funari et al., 2017; Liu et al., 2009; Wu and Ting, 2006; Wu et al., 2012) reported lower Fe content, ranging from 5.2 to 10.9 mg/g; some other studies (Bayuseno and Schmahl, 2011; Lin et al., 2003; Wan et al., 2006; Zhang et al., 2011) also reported slightly higher Fe content, ranging from 27.1 to 34.3 mg/g. In summary, most studies suggest that Fe content in municipal waste fly ash are around 20 mg/g, and it has been set to 18.8 mg/g in a modeling study (Rathod et al., 2020), being consistent with experimental results.

Fe content in the two oil fly ash samples we examined were measured to be 9.1 and 18.3 mg/g (Table S5), and the average value was determined to be 13.7 ± 4.6 mg/g. The Fe content was measured to be 15.0 mg/g for one oil fly ash sample (Celo et al., 2015), close to the value we reported. In another two studies (Agrawal et al., 2008; Sippula et al., 2014), the average Fe content was measured to be 1.98 ± 0.35 (n = 4) and 1.60 ± 1.21 mg/g (n = 14), lower than our result. In a modeling study (Rathod et al., 2020), the Fe content was set to 10 mg/g for oil fly ash, being consistent with the experimental results reported by our work and Celo et al. In addition, in our work the Fe content was measured to be 191 mg/g for one heavy oil bottom ash sample, much higher than that for oil fly ash.

S1.2.2 Fe solubility of municipal waste fly ash, oil fly ash and oil bottom ash

Fe solubility in acetate buffer (pH: 4.3) was determined to range from 0.58% to 2.41% for municipal waste fly ash (Table S5), with average and median values being 1.51 ± 0.92% and 1.54%, respectively. Few previous studies measured Fe solubility for municipal waste fly ash. Fe solubility was estimated to be <2% for municipal waste fly ash when combustion temperature exceeded 1100 K (Rathod et al., 2020), agreeing with our experimental results.

Fe solubility in acetate buffer (pH: 4.3) was determined to be 11.70% and 13.43% for the two oil fly ash samples we examined (Table S5), with an average value of 12.56 ± 0.87%. In previous work, Fe solubility was measured to be 35.7% at pH of 4.7 (Desboeufs et al., 2005) and 70% in deionized water (Schroth et al., 2009), both higher than our results. Although Fe solubility measured in different studies showed some variations, all the studies suggested that oil fly ash exhibited very high Fe solubility. Moreover, Fe solubility in acetate buffer (pH: 4.3) was measured in our work to be 25.47% for one heavy oil bottom ash. Oil fly ash was emitted by high temperature combustion but showed high Fe solubility. This is probably because heavy oil has high sulfur content, leading to the formation of sulfuric acid in combustion that can condense onto co-emitted Fe oxide particles and form highly soluble Fe sulfate (Rathod et al., 2020; Sippula et al., 2009).

Table S1. Fe content and solubility for power plant coal fly ash samples (each from a coal power plant located in a different province in China) examined in this work.

sample	Fe content (μg/g)	Fe content (mg/g)	Fe solubility (%)
1	3.65×10^4	36.5	0.013
2	2.07×10^4	20.7	0.038
3	4.41×10^4	44.1	0.028
4	2.65×10^4	26.5	0.029
5	3.44×10^4	34.4	0.008
6	2.50×10^4	25.0	0.029
7	3.82×10^4	38.2	0.128
8	10.4×10^4	103.8	0.014
9	2.35×10^4	23.5	0.028
10	3.86×10^4	38.6	0.002
11	5.37×10^4	53.7	0.134
12	3.77×10^4	37.7	0.029
13	2.41×10^4	24.1	0.018
14	3.19×10^4	31.9	0.008
15	2.41×10^4	24.1	0.057
16	2.58×10^4	25.8	0.021
17	4.59×10^4	45.9	0.073
18	2.69×10^4	26.9	0.044
19	5.57×10^4	55.7	0.036
20	3.95×10^4	39.5	0.132
21	3.50×10^4	35.0	0.021
22	6.35×10^4	63.5	0.041
23	3.97×10^4	39.7	0.146
24	4.42×10^4	44.2	0.091
25	2.41×10^4	24.1	0.013
26	4.17×10^4	41.7	0.032
27	2.31×10^4	23.1	0.020
28	5.33×10^4	53.3	0.172
29	2.23×10^4	22.3	0.070
30	2.76×10^4	27.6	0.024
31	2.17×10^4	21.7	0.024

Table S2. Fe content and solubility for domestic coal combustion aerosols examined in this work.

sample	Fe content (μg/g)	Fe solubility (%)
anthracite	32	52.04
	26	27.05
semibituminous coal	35	11.71
	45	12.66
	62	34.52
	26	100.00
bituminous coal	101	7.03
	43	43.84
	25	29.86
	42	14.26

78 **Table S3.** Fe content and solubility for steelwork fly ash samples examined in this work.

sample	Fe content (μg/g)	Fe content (mg/g)	Fe solubility (%)
1	3.47×10^{5}	346.5	0.022
2	5.47×10^{5}	546.8	0.007
3	4.46×10^{5}	446.2	0.022
4	4.34×10^{5}	434.0	0.012
5	9.79×10^{4}	97.9	0.069
6	1.34×10^{4}	13.4	6.928
7	1.28×10^{4}	12.8	0.191
8	2.09×10^{4}	20.9	0.395
9	6.45×10^{5}	644.9	0.011
10	2.13×10^{5}	213.1	4.024
11	5.66×10^{5}	565.6	3.126
12	3.94×10^{5}	393.8	1.980
13	4.48×10^{5}	448.3	0.042
14	2.59×10^{4}	25.9	0.923
15	9.74×10^{4}	97.4	10.640
16	1.97×10^{5}	197.1	0.055
17	3.03×10^{5}	302.8	0.035
18	5.97×10^{5}	596.8	0.010
19	4.73×10^{5}	472.7	0.022
20	4.04×10^{5}	404.3	0.014
21	7.32×10^{5}	732.2	0.013
22	3.58×10^{4}	35.8	0.158
23	9.19×10^{5}	918.9	8.589
24	4.46×10^{5}	446.2	0.050
25	5.81×10^{3}	5.8	1.983
26	6.07×10^{5}	607.4	0.180
27	2.60×10^{4}	26.0	0.068
28	5.80×10^{3}	5.8	0.158
29	7.38×10^{3}	7.4	0.064

79

80

81

Table S4. Fe content and solubility for biofuel burning aerosols examined in this work.

sample	Fe content (μg/g)	Fe solubility (%)
wheat	21	60.14
	8	100.00
	6	26.09
	12	71.87
rice	n. a.	40.52
	28	47.06
	20	4.34
corn	3	44.83
	2	100.00
	3	100.00
	15	77.52
	7	88.36
rape	70	54.34
	6	57.39
cogongrass	11	89.41
	10	85.33
	19	86.46
	71	37.56
China fir	3	5.75
	3	43.64
	12	20.01
pine	72	67.55
	101	100.00
	40	65.91
poplar	18	2.86
pine needle	13	24.01
	21	27.06
	15	41.86

Table S5. Fe content and solubility for municipal waste fly ash, oil fly ash and oil bottom ash samples examined in this work. WP-2 is a fly ash sample obtained from an electrostatic precipitator in a waste incineration plant in Shanghai, China (Li et al., 2021), and BCR-176R and BCR-615 are certified reference materials provided by the Institute for Reference Materials and Measurements.

sample	Fe content (μg/g)	Fe content (mg/g)	Fe solubility (%)
municipal waste fly ash			
WP-2	3.87×10^{3}	3.9	0.58
BCR-176R	2.26×10^{4}	22.6	2.41
BCR-615	2.97×10^{4}	29.7	1.54
oil bottom ash	1.91×10^{5}	191.5	25.47
oil fly ash			
diesel oil	1.83×10^{4}	18.3	11.70
heavy fuel oil	9.06×10^{3}	9.1	13.43

Table S6. Summary of Fe content (mg/g) for anthropogenic and combustion aerosol Fe determined in our present study and previous work (*n*: number of samples examined).

sample type	size range	*n*	range	average	median	Reference
power plant		31	20.7-103.8	37.2±16.8	35.0	This work
coal fly ash		3	16.0-52.0	33.0±18.0	31.0	Baldo et al. (2021)
		7	21.8-205.1	65.9±67.4	34.4	Goodarzi (2006)
		1		46.7		Meij (1994)
		23	18.2-112.0	57.8±22.7	52.5	Moreno et al. (2005)
		4	7.7-97.3	54.3±39.5	56.0	Jankowski et al. (2006)
		4	58.9-101.0	81.1±19.4	82.3	Dutta et al. (2009)
		4	27.0-119.0	86.0±43.0	97.5	Fu et al. (2012)
		7	38.3-98.6	62.1±26.7	43.2	Li et al. (2022)
domestic coal	$PM_{2.5}$	10	0.025-0.101	0.044±0.023	0.038	This work
combustion aerosol	$PM_{2.5}$	3		0.048±0.035		Patil et al. (2013)
	$PM_{2.5}$	4		0.671±0.023		Watson et al. (2001)
	$PM_{2.5}$	5		0.7±0.1		Zhang et al. (2012)
	PM_{10}	3		0.061±0.044		Patil et al. (2013)
steelwork fly ash		29	5.8-918.9	312.6±246.1	346.5	This work
		1		358.9		Souza et al. (2010)
		1		369.3		Vieira et al. (2013)
		1		312.2		Silva et al. (2019)
		4	288.2-340.3	329.1±22.6	324.4	Alizadeh and Momeni (2016)
			280-380			Hagni et al. (1991)
		1		86.0		Stathopoulos et al. (2013)
		1		128.1		Xia and Picklesi (2000)

		1		150.8		Loaiza et al. (2017)
		1		286.5		Laforest and Duchesne (2006)
		1		284.6		Alsheyab and Khedaywi (2016)
		1		238.7		Li et al. (2023)
		4	234.1-361.1	267.3±4.8	283.6	Al-Negheimish et al. (2021)
		1		489.6		Machado et al. (2006)
		2	430-470	450±20	450	Patil et al. (2013)
		10	8.2-720			Hleis et al. (2013)
		1		515.0		Ye et al. (2021)
Biofuel burning aerosol	$PM_{2.5}$	27	0.002-0.101	0.023±0.026	0.013	This work
	$PM_{2.5}$	3		0.024±0.017		Patil et al. (2013)
	PM_2	2		0.090	0.090	Hildemann et al. (1991)
	$PM_{2.5}$	3		0.167±0.259		Watson et al. (2001)
	$PM_{2.5}$	4		0.180±0.196		Watson et al. (2001)
	$PM_{2.5}$	5	0.031-0.615	0.162	0.115	Hedberg et al. (2002)
	$PM_{2.5}$	1		0.440		Alves et al. (2011)
	$PM_{2.5}$	4		0.400±0.100		Zhang et al. (2012)
	PM_{10}	4	0.250-1.70	0.723±0.661	0.470	Schmidl et al. (2008)
municipal waste fly ash		3	3.9-29.7	18.7±13.3	22.6	This work
		3	7.8-33	18.0±13.3	13.2	Raclavská et al. (2017)
		1		23.1		Cobo et al. (2009)
		1		5.2		Wu and Ting (2006)
		1		5.5		Funari et al. (2017)
		1		10.5		Wu et al. (2012)
		1		10.9		Liu et al. (2009)
		1		29.4		Zhang et al. (2011)
		1		33.8		Wan et al. (2006)

	1		34.3		Lin et al. (2003)
	1		37.1		Bayuseno and Schmahl (2011)
oil fly ash	2	9.1-18.3	13.7±4.6	13.7	This work
	7		15.0		Celo et al. (2015)
	4	1.55-2.36	1.98±0.35	2.10	Agrawal et al. (2008)
	14	0.331-4.46	1.60±1.21	1.16	Sippula et al. (2014)
oil bottom ash	1		191	191	This work

94

Table S7. Summary of Fe solubility (%) for anthropogenic and combustion aerosol Fe determined in our present study and previous work (*n*: number of samples examined; pH: acidity of the leaching solution).

sample type	size range	*n*	pH	range	average	median	Reference
power plant		31	4.3	0.002-0.17	0.05±0.05	0.03	This work
coal fly ash		1	~6		0.06		Oakes et al. (2012)
		1	~4.7		0.2		Desboeufs et al. (2005)
		7	4.3	0.09-0.87	0.24±0.28	0.13	Li et al. (2022)
		7	~6	0.02-0.75	0.16±0.26	0.06	Li et al. (2022)
domestic coal combustion aerosol		10	4.3	7.03-100	33.30±27.71	28.45	This work
steelwork fly ash		29	4.3	0.007-10.64	1.37±2.77	0.07	This work
biofuel burning aerosol		28	4.3	2.86-100	56.07±30.95	55.87	This work
municipal waste fly ash		3	4.3	0.58-2.41	1.51±0.92	1.54	This work
oil fly ash		2	4.3	11.70-13.43	12.56±0.87	12.56	This work
		1	4.7		35.7		Desboeufs et al. (2005)
		1	~6		70%		Schroth et al. (2009)
oil bottom ash		1	4.3		25.47%		This work

S2 Modeling methods and results

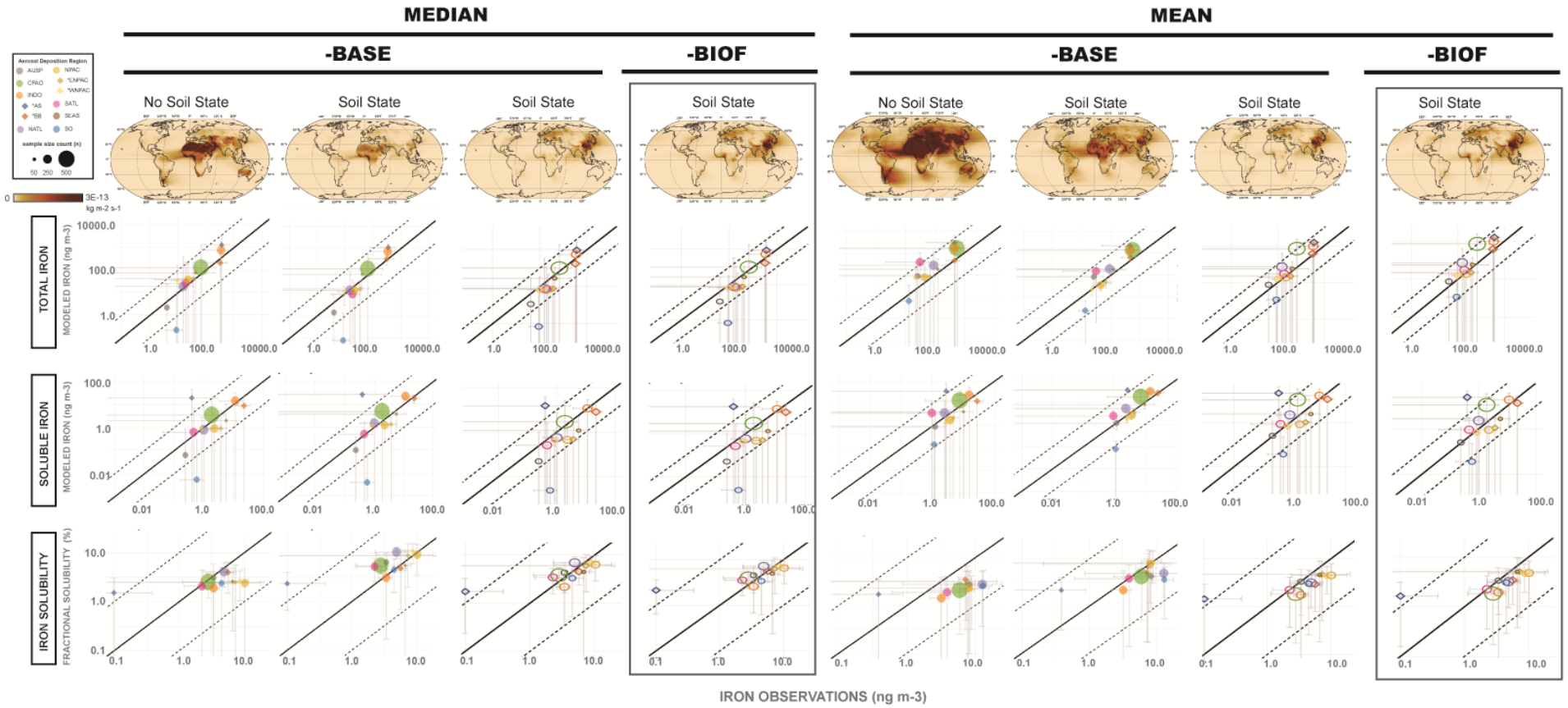

Figure S3. Model-observation comparisons (n = 1624) of surface aerosol Fe concentrations using two different dust flux schemes (soil state submodule included versus no soil state submodule). Open and solid circles indicate use of the central- and high-residential emission inventories, respectively, and the box indicates MIMI v1.1. Model skill was best when the soil state scheme was used, -BIOF solubility parameters were applied,

the central-residential emissions inventory was used, and both modeled and observed aerosol Fe concentrations were aggregated over time and space by medians when compared to means.

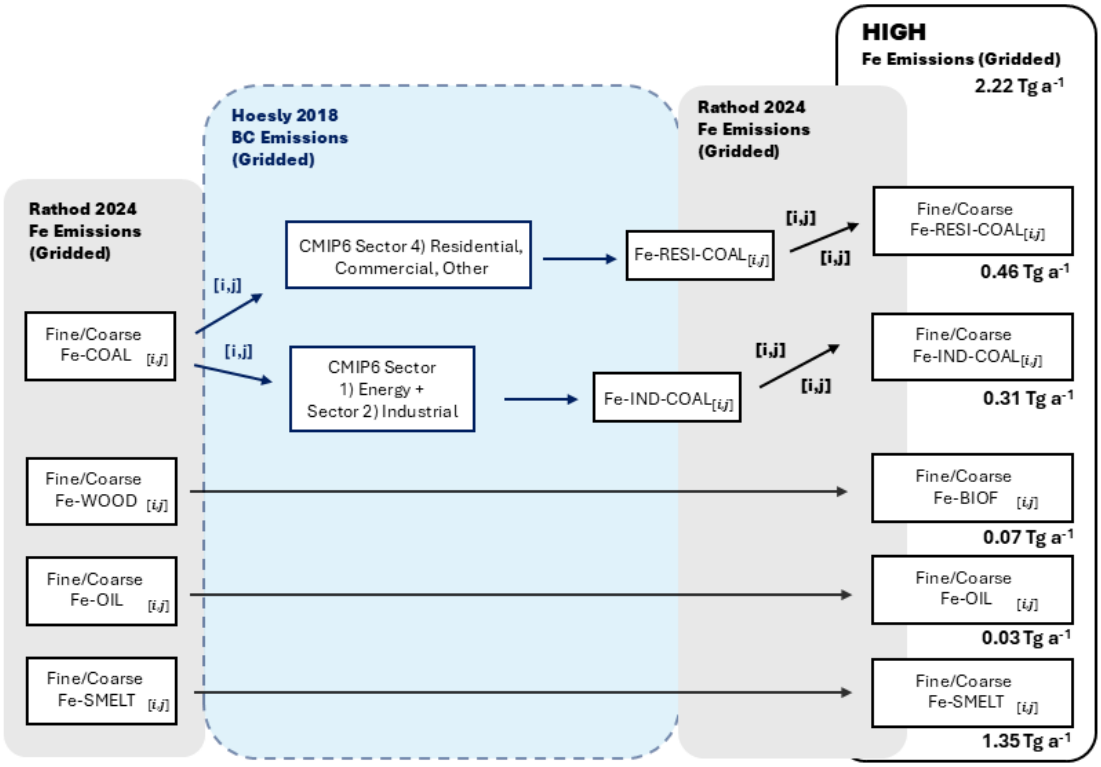

Figure S4. A flowchart representing the steps followed and datasets leveraged to create the **high**-combustion Fe emissions inventory. Dashed outlines indicate a BC dataset; solid/no outlines indicate an Fe dataset; [i,j] indicates that the fractional split was grid-cell dependent; above/below the arrow indicates the fine/coarse fraction, respectively.

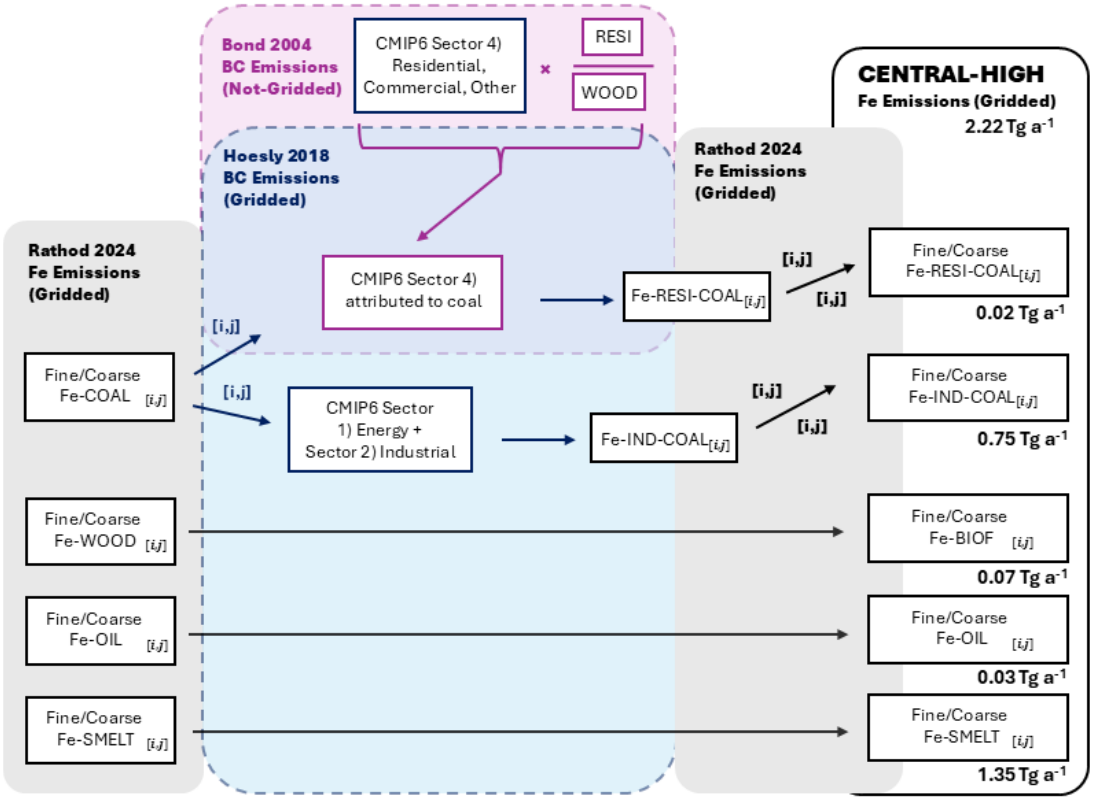

Figure S5. A flowchart representing the steps followed and datasets leveraged to create the **central-high**-combustion Fe emissions inventory. Dashed outlines indicate a BC dataset; solid/no outlines indicate an Fe dataset; [i,j] indicates that the fractional split was grid-cell dependent; above/below the arrow indicates the fine/coarse fraction, respectively.

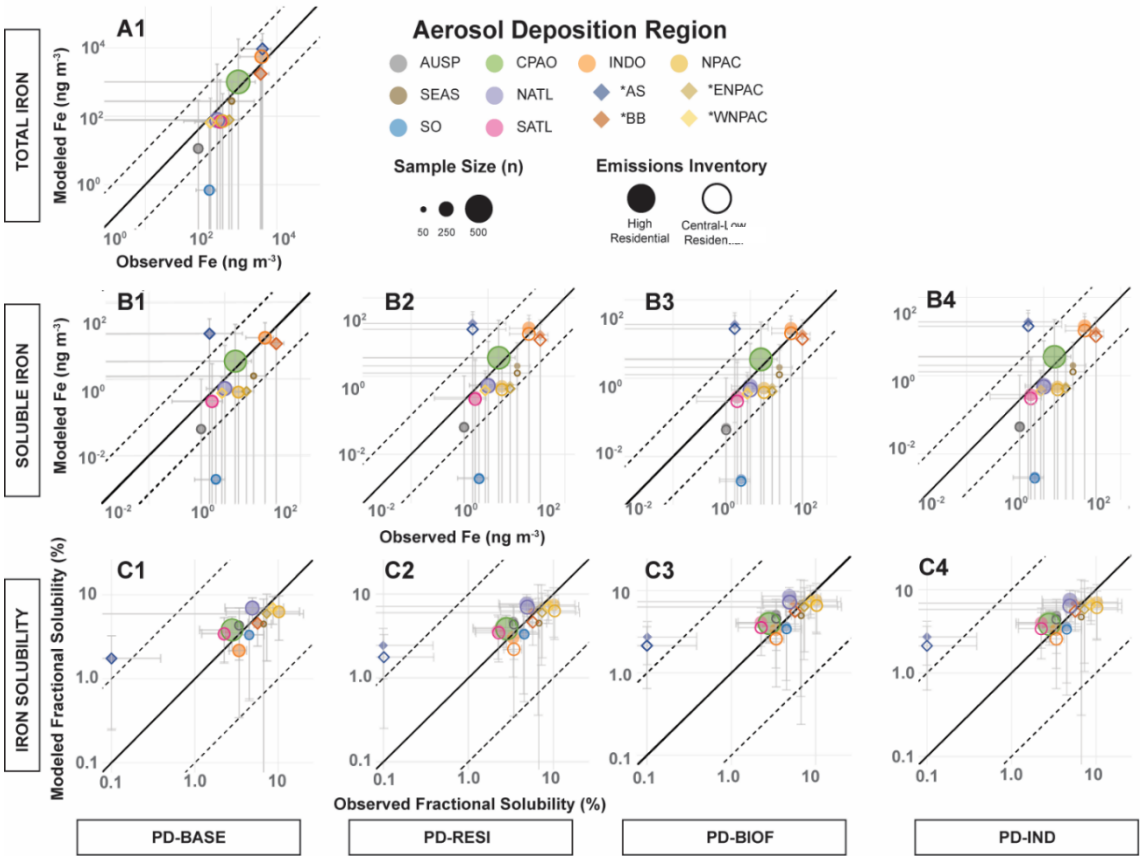

Figure S6. Comparison of modelling and observational data including results from the PD-IND run, which altered oil and industrial coal solubility parameters (industrial coal Fe solubility from 0.2 to 0.05% and oil from 38 to 25%). Error bars represent spatiotemporal variance within each region. The solid black line indicates a 1-to-1 relationship and the dashed lines represent deviation by ±1 order of magnitude.

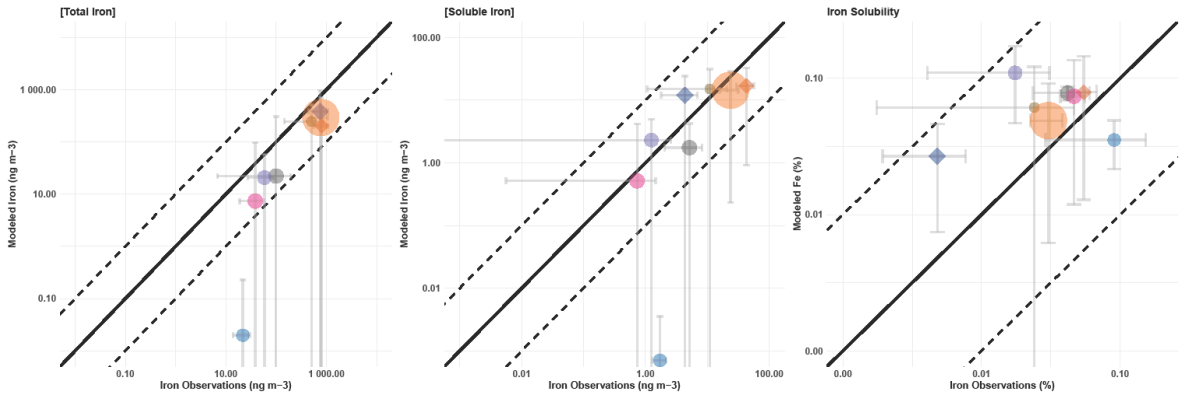

Figure S7. Model-observation comparisons (n = 25) of surface aerosol Fe concentrations using the high-residential emissions inventory for the model simulations and only using observations co-located in regions where soluble Fe fluxes increased by a factor of 2 using the PD-BIOF solubility parameters in attempt to isolate observations most representative of residential coal and biofuel aerosol.

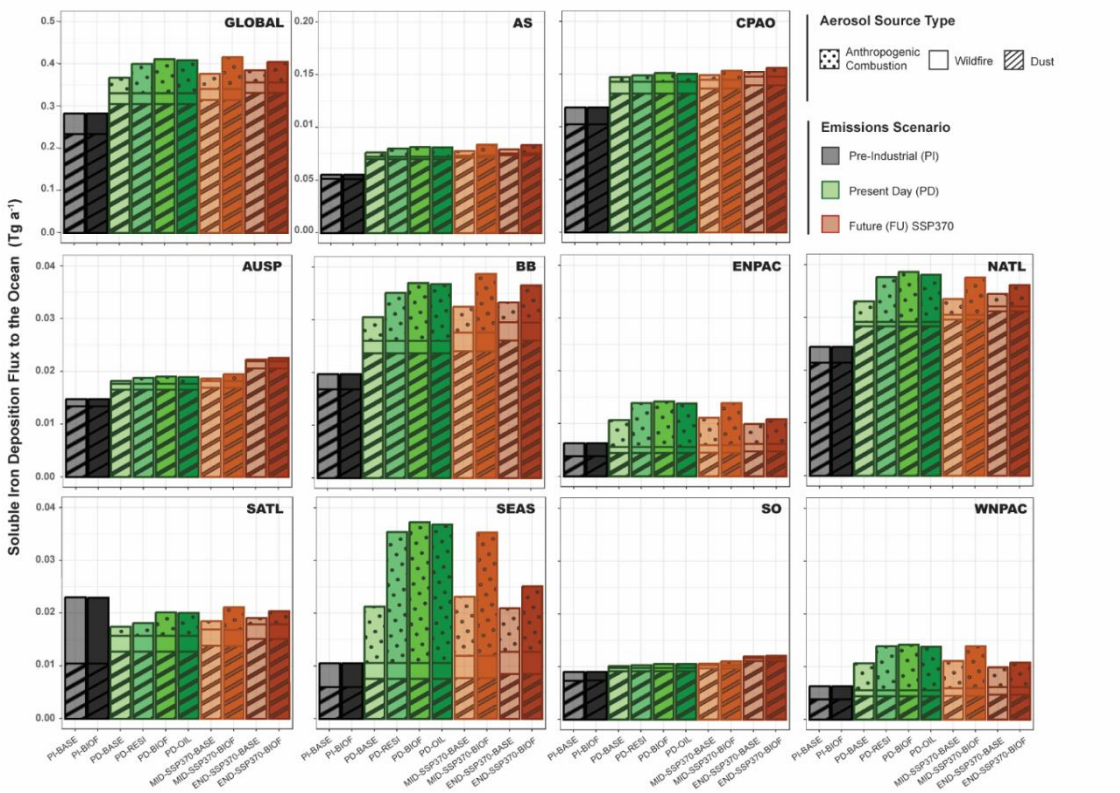

137

138 **Figure S8.** Deposition fluxes of soluble aerosol Fe to marine ecosystems globally and in

139 regional grouping with inclusion of the PD-IND (labeled PD-OIL in this figure) simulations.

140 Fluxes are source-apportioned (dust, biofuel burning, and anthropogenic combustion) and

141 provided for each model simulation.

142

143

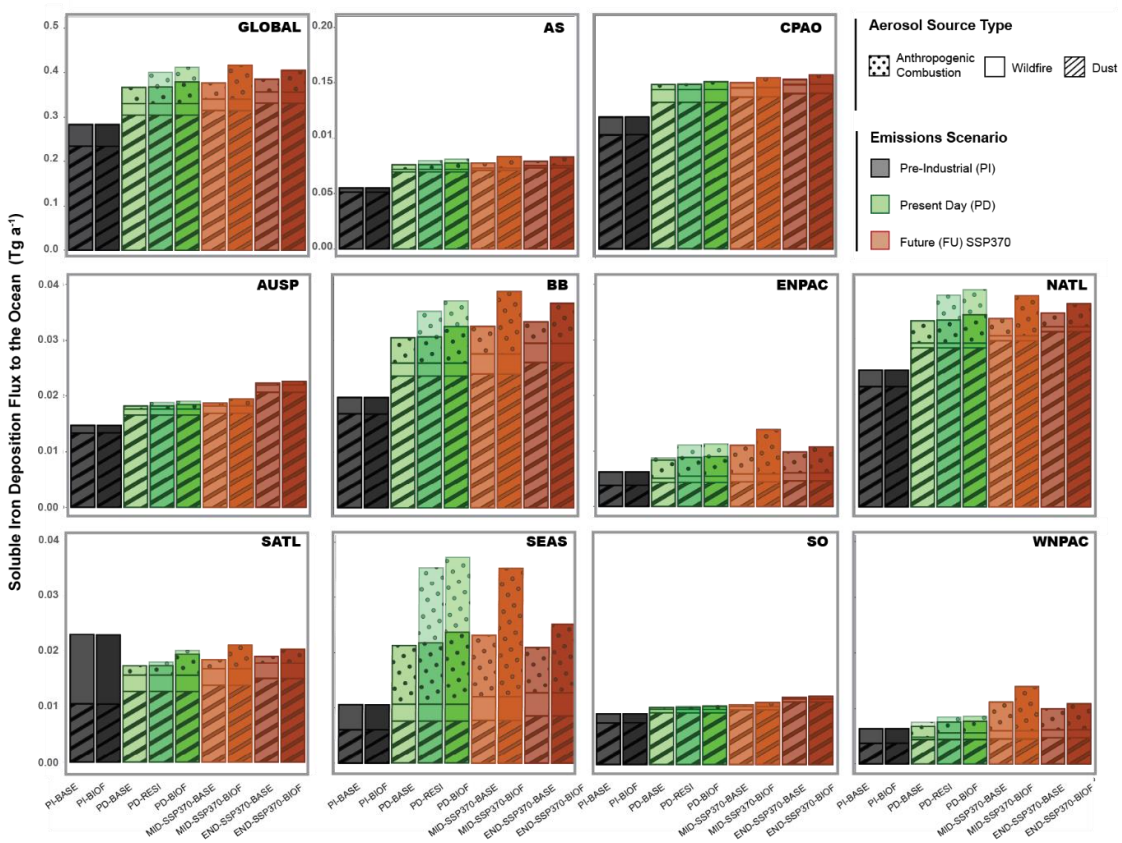

Figure S9. Deposition fluxes of soluble aerosol Fe to marine ecosystems globally and in regional grouping with inclusion of the simulations that utilized the central-high residential emissions inventory. Fluxes are source-apportioned (dust, biofuel burning, and anthropogenic combustion) and provided for each model simulation. For the PD, transparent bars represent the high-residential emissions inventory and opaque represent the central-high.

Table S8. Distinctions in fuel- and sector-type information pertaining to combustion emissions in the literature applied in this work to estimate residential combustion emissions of iron. n.d. = not determined.

	Rathod et al., 2020	Hoesly et al., 2018	Bond et al., 2004	This work
Chemical Species	Iron	Black Carbon	Black Carbon	Iron
Fuel-Type	Coal, Biofuels	n.d.	Coal, Biofuels	Coal, Biofuels
Sector	Industrial, Residential	Industrial, Residential	Industrial, Residential	Industrial, Residential
Gridding	Only at fuel level	Only at sector level	n.d.	At fuel and sector level

Table S9. Final breakdown of Fe and Black Carbon (BC) emissions by sector (fuel-type) as represented in the three Fe emissions inventories developed and tested in this work. Emission fluxes are reported in Gg a^{-1} with three significant figures.

	Central-Residential-Case		**Central-High-Residential-Case**		**High Residential-Case**	
Fuel-Type	**Iron**	**Black Carbon**	**Iron**	**Black Carbon**	**Iron**	**Black Carbon**
Residential Coal	4.88	1060	16.3	2160	464	2160
Industrial Coal	765	1720	753	1720	305	1720
Oil (shipping/transportation)	34.5	1250	34.5	1250	34.5	1250
Residential Biofuel	70.6	2400	71.5	1330	71.5	1330
Waste	0.92	551	n.d.	n.d.	n.d.	n.d.
Smelting	1350	n.d.	1350	n.d.	1350	n.d.
TOTAL	**2220**	**6970**	**2220**	**6460**	**2220**	**6460**

Table S10. Fe deposition flux budgets (Gg a^{-1}; to two significant figures) for each key marine region utilizing the **high-**residential emissions inventory. Values reported herein only include fluxes to marine systems (model grid cells where ocean fraction > 50%). AS: Arabian Sea, CPAO: Central Pacific and Atlantic Ocean, AUSP: Australia and South Pacific, BB: Bay of Bengal, ENPAC: Eastern North Pacific, NATL: North Atlantic, SATL: South Atlantic, SEAS: Southeastern Asia, SO: Southern Ocean, WNPAC: Western North Pacific.

	Simulation	**Region**												
		Global	**SATL**	**NATL**	**AS**	**BB**	**INDO**	**SEAS**	**ENPAC**	**WNPAC**	**ARCT**	**AUSP**	**SO**	**CPAO**
Total Fe	PD-BASE	23000	1300	2200	6700	1500	8300	700	170	120	60	1200	600	8700
Total Anth. Fe	PD-BASE	590	24	72	57	65	120	240	43	19	9.3	11	5.3	39
Soluble Fe	PD-BASE	370	17	33	76	31	110	21	6.6	4.2	2.0	18	10	150
	PD-RESI	400	18	38	80	35	120	35	9.0	5.1	2.4	19	10	150
	PD-BIOF	410	20	39	81	37	120	37	9.1	5.3	3.0	19	11	150
	PD-IND	410	20	38	81	37	120	37	9.0	5.0	2.4	19	10	150
Soluble Anth. Fe	PD-BASE	36	1.7	3.9	4.2	4.5	8.7	11	3.3	1.9	0.6	0.5	0.3	4.7
	PD-RESI	70	2.4	8.5	7.8	9.2	17	25	5.6	2.9	1.0	1.2	0.5	5.9
	PD-BIOF	81	4.4	9.4	9.3	11	20	27	5.8	3.0	1.1	1.4	0.7	8.1
	PD-IND	78	4.4	8.9	9.1	11	20	26	5.6	2.8	1.0	1.3	0.7	7.6

Table S11. Fe deposition flux budgets (Gg a^{-1}; to two significant figures) for each key marine region utilizing the **central-high**-residential emissions inventory. Values reported herein only include fluxes to marine systems (model grid cells where ocean fraction > 50%).

	Simulation	**Region**												
		Global	**SATL**	**NATL**	**AS**	**BB**	**INDO**	**SEAS**	**ENPAC**	**WNPAC**	**ARCT**	**AUSP**	**SO**	**CPAO**
Total Fe	PD-BASE	23000	1300	2200	6700	1500	8200	710	170	120	59	1200	600	8600
Total Anth. Fe	PD-BASE	590	24	72	57	65	120	240	43	19	9.3	11	5.3	39
Soluble Fe	PD-BASE	370	17	33	76	30	110	21	6.6	4.2	2.0	18	10	150
	PD-RESI	370	17	33	76	31	110	22	6.7	4.2	2.0	18	10	150
	PD-BIOF	380	19	34	78	32	110	24	6.9	4.3	2.1	18	10	150
Soluble Anth. Fe	PD-BASE	36	1.7	3.9	4.2	4.5	8.7	11	3.3	1.9	0.6	0.5	0.3	4.7
	PD-RESI	37	1.7	4.1	4.3	4.7	9.0	11	3.3	1.9	0.6	0.6	0.3	4.7
	PD-BIOF	49	3.8	5.0	5.7	6.5	12	13	3.5	2.1	0.7	0.8	0.5	6.9

Table S12. Fe deposition flux budgets (Gg a^{-1}; to two significant figures) for each key marine region utilizing the **central**-residential emissions inventory. Values reported herein only include fluxes to marine systems (model grid cells where ocean fraction > 50%).

	Simulation	**Region**												
		Global	**SATL**	**NATL**	**AS**	**BB**	**INDO**	**SEAS**	**ENPAC**	**WNPAC**	**ARCT**	**AUSP**	**SO**	**CPAO**
Total Fe	PD-BASE	23000	1300	2200	6700	1500	8200	710	170	120	59	1200	600	8600
Total Anth. Fe	PD-BASE	610	25	68	61	70	130	250	41	20	9.3	10	5.4	54
Soluble Fe	PD-BASE	370	17	33	76	30	110	21	6.5	4.1	2.0	18	10	150
	PD-RESI	370	17	33	76	30	110	21	6.5	4.2	2.0	18	10	150
	PD-BIOF	380	17	33	78	32	110	23	7.0	4.4	2.0	18	10	150
Soluble Anth. Fe	PD-BASE	36	1.2	3.8	4.3	4.5	8.8	10	3.1	1.9	0.60	0.51	0.30	5.1
	PD-RESI	36	1.2	3.8	4.3	4.6	8.9	11	3.1	1.9	0.60	0.52	0.30	5.2
	PD-BIOF	46	1.5	4.4	5.9	6.4	12	13	3.6	2.1	0.65	0.67	0.40	7.2

Table S13. Root Mean Square Error (RMSE) as a measure of difference between observed and modeled values for total and soluble Fe (ng m^{-3}) and Fe solubility, grouped by marine region and aggregated by median. The case with the -BIOF solubility parameterization, with the soil state module, and the central-residential emissions inventory represent MIMI v1.1. Values reported reflect three significant figures.

		-BIOF	**-BASE**		
		With Soil State (Central)	**With Soil State (Central)**	**With Soil State (High Residential)**	**Without Soil State**
Total Fe	AS	1300	1300	1300	4050
Soluble Fe	AS	21.2	18.2	18.2	45.2
Solubility	AS	0.021	0.016	0.017	0.010
Total Fe	AUSP	61.4	61.4	59.7	258
Soluble Fe	AUSP	2.12	2.128	2.12	1.82
Solubility	AUSP	0.112	0.113	0.113	0.120
Total Fe	BB	356	356	363	238
Soluble Fe	BB	22.6	25.6	25.5	22.4
Solubility	BB	0.064	0.066	0.066	0.070
Total Fe	CPAO	1300	1300	1300	3320
Soluble Fe	CPAO	17.1	17.1	17.1	20.7
Solubility	CPAO	0.151	0.151	0.151	0.150
Total Fe	ENPAC	95.7	95.7	95.7	86.7
Soluble Fe	ENPAC	5.81	5.83	5.83	4.86
Solubility	ENPAC	0.080	0.080	0.080	0.080
Total Fe	NATL	203	203	202	582
Soluble Fe	NATL	3.84	3.85	3.85	3.68
Solubility	NATL	0.249	0.250	0.250	0.260
Total Fe	SATL	122	122	122	1250
Soluble Fe	SATL	1.83	1.85	1.84	4.16
Solubility	SATL	0.039	0.040	0.039	0.040
Total Fe	SEAS	172	172	173	160
Soluble Fe	SEAS	13.6	13.8	13.8	12.1
Solubility	SEAS	0.064	0.063	0.064	0.065
Total Fe	SO	19.7	19.7	19.7	21.2
Soluble Fe	SO	1.76	1.76	1.76	1.62
Solubility	SO	0.225	0.226	0.226	0.227
Total Fe	WNPAC	35.2	35.2	35.2	71.9
Soluble Fe	WNPAC	4.60	4.61	4.61	4.34
Solubility	WNPAC	0.051	0.051	0.051	0.080

Table S14. Summary statistics for model (Mod)-observation (Obs) comparisons of soluble Fe. RMSE: root mean square error, SD: standard deviation. ΔRMSE represents comparison between the base simulation (PD-BASE) and each sensitivity case using the high-residential emissions inventory as an upper constraint. Values are reported to two significant figures.

		Median Surface Concentration ($ng\ m^{-3}$)		Mean Surface Concentration ± SD ($ng\ m^{-3}$)			
Model Case	**Region**	**Obs**	**Mod**	**Obs**	**Mod**	**Δ Obs – Mod median**	**Δ RMSE**
PD-BASE	AS	0.40	15	2.7 ± 4.6	16 ± 8.3	-15	NA
PD-RESI			22		23 ± 14	-22	11
PD-BIOF			23		26 ± 17	-23	15
PD-IND			23		25 ± 17	-23	15
PD-BASE	AUSP	0.24	0.05	1.1 ± 2.2	0.19 ± 0.4	0.19	NA
PD-RESI			0.05		0.37 ± 0.92	0.19	-0.18
PD-BIOF			0.05		0.44 ± 1.15	0.19	-0.06
PD-IND			0.05		0.44 ± 1.13	0.19	-0.06
PD-BASE	BB	23	8.6	27 ± 20	8.4 ± 4.8	14	NA
PD-RESI			11		13 ± 10	11	-4.7
PD-BIOF			13		15 ± 12	9.4	-6.3
PD-IND			13		15 ± 12	9.4	-6.2
PD-BASE	CPAO	1.9	2.9	7.3 ± 18	6.3 ± 7.3	-0.99	NA
PD-RESI			3.0		6.3 ± 7.3	-1.1	0.00
PD-BIOF			3.1		6.4 ± 7.4	-1.2	0.00
PD-IND			3.1		6.4 ± 7.4	-1.1	0.00
PD-BASE	ENPAC	3.8	0.48	4.6 ± 4.3	0.53 ± 0.19	3.3	NA
PD-RESI			0.60		0.67 ± 0.27	3.2	-0.10
PD-BIOF			0.60		0.68 ± 0.28	3.1	-0.11
PD-IND			0.56		0.63 ± 0.26	3.2	-0.07
PD-BASE	NATL	1.0	0.56	2.3 ± 3.5	0.85 ± 1.1	0.45	NA
PD-RESI			0.60		1.1 ± 1.9	0.41	0.03
PD-BIOF			0.62		1.2 ± 2	0.38	0.03
PD-IND			0.57		1.1 ± 1.9	0.44	0.04
PD-BASE	SATL	0.46	0.27	0.95 ± 2.3	0.4 ± 0.65	0.19	NA
PD-RESI			0.29		0.42 ± 0.69	0.18	-0.03
PD-BIOF			0.33		0.5 ± 0.79	0.13	-0.05
PD-IND			0.32		0.49 ± 0.78	0.14	-0.05
PD-BASE	SEAS	5.8	1.19	9.8 ± 11	1.3 ± 1.1	4.6	NA
PD-RESI			1.81		2.3 ± 2.8	4.0	-0.43
PD-BIOF			1.87		2.3 ± 2.9	3.9	-0.47
PD-IND			1.80		2.2 ± 2.8	4.0	-0.43
PD-BASE	SO	0.59	0.00	1.1 ± 1.4	0.01 ± 0.03	0.58	NA
PD-RESI			0.00		0.01 ± 0.03	0.58	0.00
PD-BIOF			0.0		0.01 ± 0.03	0.58	0.00
PD-IND			0.0		0.01 ± 0.02	0.58	0.00

PD-BASE	WNPAC	0.85	0.42	2.7 ± 4.1	0.41 ± 0.03	0.42	NA
PD-RESI			0.49		0.47 ± 0.03	0.36	-0.02
PD-BIOF			0.50		0.48 ± 0.03	0.35	-0.03
PD-IND			0.46		0.42 ± 0.02	0.39	0.00

189

Table S15. Summary statistics for model (Mod)-observation (Obs) comparisons of soluble Fe. RMSE: root mean square error, SD: standard deviation. ΔRMSE represents comparison between the base simulation (PD-BASE) and each sensitivity case using the **central**-residential emissions inventory as a lower constraint. Values are reported to two significant figures.

		Median Surface Concentration ($ng\ m^{-3}$)		Mean Surface Concentration ± SD ($ng\ m^{-3}$)			
Model Case	**Region**	**Obs**	**Mod**	**Obs**	**Mod**	**Δ Obs – Mod median**	**Δ RMSE**
PD-BASE	AS	0.40	15.5	2.69 ± 4.59	16 ± 8.3	-15	NA
PD-RESI			15.6		16 ± 8.3	-15	0.09
PD-BIOF			18.3		19 ± 8.8	-18	3.0
PD-IND			18.1		19 ± 8.7	-18	2.8
PD-BASE	AUSP	0.24	0.05	1.13 ± 2.20	0.19 ± 0.39	0.2	NA
PD-RESI			0.05		0.19 ± 0.4	0.2	0.00
PD-BIOF			0.05		0.25 ± 0.61	0.2	-0.01
PD-IND			0.05		0.24 ± 0.59	0.2	0.00
PD-BASE	BB	22.76	8.2	27.03 ± 20.1	8.2 ± 4.8	14.5	NA
PD-RESI			8.3		8.4 ± 4.9	14.4	-0.1
PD-BIOF			10		11 ± 7.9	12.7	-3.0
PD-IND			9.9		11 ± 7.8	12.8	-2.9
PD-BASE	CPAO	1.91	2.9	7.28 ± 18.1	6.3 ± 7.4	-1.0	NA
PD-RESI			2.9		6.3 ± 7.4	-1.0	0.00
PD-BIOF			3.0		6.4 ± 7.4	-1.1	0.01
PD-IND			3.0		6.3 ± 7.4	-1.1	0.01
PD-BASE	ENPAC	3.75	0.48	4.63 ± 4.25	0.53 ± 0.2	3.3	NA
PD-RESI			0.48		0.5 ± 0.18	3.3	0.00
PD-BIOF			0.50		0.6 ± 0.2	3.3	-0.03
PD-IND			0.47		0.5 ± 0.19	3.3	0.01
PD-BASE	NATL	1.01	0.56	2.34 ± 3.52	0.86 ± 1.2	0.4	NA
PD-RESI			0.56		0.87 ± 1.2	0.4	0.00
PD-BIOF			0.58		0.99 ± 1.5	0.4	-0.01
PD-IND			0.51		0.88 ± 1.4	0.5	0.02
PD-BASE	SATL	0.46	0.26	0.95 ± 2.25	0.38 ± 0.63	0.2	NA
PD-RESI			0.26		0.38 ± 0.63	0.2	0.00
PD-BIOF			0.27		0.4 ± 0.65	0.2	-0.02
PD-IND			0.26		0.39 ± 0.65	0.2	-0.01
PD-BASE	SEAS	5.77	1.2	9.80 ± 11.2	1.3 ± 1.1	4.6	0 NA
PD-RESI			1.2		1.3 ± 1.1	4.6	-0.01
PD-BIOF			1.3		1.5 ± 1.4	4.4	-0.12
PD-IND			1.2		1.4 ± 1.3	4.5	-0.07
PD-BASE	SO	0.59	0.00	1.12 ± 1.4	0.01 ± 0.01	0.6	NA
PD-RESI			0.00		0.01 ± 0.01	0.6	0.00
PD-BIOF			0.00		0.01 ± 0.01	0.6	0.00
PD-IND			0.00		0.01 ± 0.01	0.6	0.00

PD-BASE	WNPAC	0.85	0.42	2.67 ± 4.06	0.41 ± 0.12	0.4	NA
PD-RESI			0.43		0.41 ± 0.12	0.4	0.00
PD-BIOF			0.45		0.43 ± 0.12	0.4	-0.01
PD-IND			0.40		0.38 ± 0.12	0.4	0.02

194

Table S16. Summary statistics for model (Mod)-observation (Obs) comparisons of Fe solubility. RMSE: root mean square error, SD: standard deviation. ΔRMSE represents comparison between the base simulation (PD-BASE) and each sensitivity case using the **high-**residential emissions inventory as an upper constraint. Values are reported to two significant figures.

		Median Surface Solubility		Mean Surface Fractional Solubility ± SD			
Model Case	**Region**	**Obs**	**Mod**	**Obs**	**Mod**	**Δ Obs – Mod median**	**Δ RMSE**
PD-BASE	AS	0.001	0.02	0.004	0.02 ± 0.01	-0.02	0.00
PD-RESI			0.02		0.03 ± 0.01	-0.02	0.01
PD-BIOF			0.03		0.03 ± 0.01	-0.03	0.02
PD-IND			0.03		0.03 ± 0.01	-0.03	0.02
PD-BASE	AUSP	0.03	0.04	0.08	0.04 ± 0.01	-0.01	0.00
PD-RESI			0.05		0.05 ± 0.01	-0.01	0.00
PD-BIOF			0.05		0.06 ± 0.01	-0.02	0.00
PD-IND			0.05		0.05 ± 0.01	-0.02	0.00
PD-BASE	BB	0.06	0.05	0.07	0.04 ± 0.01	0.01	0.00
PD-RESI			0.06		0.06 ± 0.01	-0.01	0.00
PD-BIOF			0.07		0.07 ± 0.01	-0.01	0.00
PD-IND			0.07		0.07 ± 0.01	-0.01	0.00
PD-BASE	CPAO	0.03	0.04	0.06	0.04 ± 0.03	-0.01	0.00
PD-RESI			0.04		0.04 ± 0.03	-0.01	0.00
PD-BIOF			0.04		0.05 ± 0.03	-0.01	0.00
PD-IND			0.04		0.05 ± 0.03	-0.01	0.00
PD-BASE	ENPAC	0.07	0.06	0.08	0.07 ± 0.02	0.01	0.00
PD-RESI			0.07		0.09 ± 0.02	0.00	0.00
PD-BIOF			0.07		0.09 ± 0.02	0.00	0.00
PD-IND			0.07		0.08 ± 0.02	0.00	0.00
PD-BASE	NATL	0.05	0.07	0.12	0.07 ± 0.02	-0.02	0.00
PD-RESI			0.08		0.08 ± 0.02	-0.03	0.00
PD-BIOF			0.09		0.09 ± 0.02	-0.04	0.00
PD-IND			0.08		0.08 ± 0.02	-0.03	0.00
PD-BASE	SATL	0.02	0.03	0.04	0.03 ± 0.01	-0.01	0.00
PD-RESI			0.04		0.04 ± 0.01	-0.01	0.00
PD-BIOF			0.04		0.04 ± 0.01	-0.02	0.00
PD-IND			0.04		0.04 ± 0.01	-0.02	0.00
PD-BASE	SEAS	0.07	0.04	0.07	0.06 ± 0.04	0.02	0.00
PD-RESI			0.07		0.09 ± 0.04	0.00	0.00
PD-BIOF			0.07		0.09 ± 0.04	0.00	0.00
PD-IND			0.07		0.08 ± 0.03	0.00	-0.01
PD-BASE	SO	0.05	0.03	0.13	0.03 ± 0.01	0.01	0.00
PD-RESI			0.03		0.04 ± 0.01	0.01	0.00
PD-BIOF			0.04		0.04 ± 0.01	0.01	0.00

PD-IND			0.04		0.04 ± 0.01	0.01	0.00
PD-BASE	WNPAC	0.09	0.07	0.09	0.08 ± 0.03	0.02	0.00
PD-RESI			0.08		0.09 ± 0.03	0.01	0.00
PD-BIOF			0.08		0.09 ± 0.03	0.00	0.00
PD-IND			0.07		0.08 ± 0.02	0.01	0.00

200

Table S17. Summary statistics for model (Mod)-observation (Obs) comparisons of Fe solubility. RMSE: root mean square error, SD: standard deviation. ΔRMSE represents comparison between the base simulation (PD-BASE) and each sensitivity case using the **central-**residential emissions inventory as an upper constraint. Values are reported to two significant figures.

		Median Surface Solubility		Mean Surface Fractional Solubility ± SD			
Model Case	**Region**	**Obs**	**Mod**	**Obs**	**Mod**	**Δ Obs – Mod median**	**Δ RMSE**
PD-BASE	AS	0.001	0.02	0.004	0.02 ± 0.01	-0.02	0.00
PD-RESI			0.02		0.02 ± 0.01	-0.02	0.00
PD-BIOF			0.02		0.02 ± 0.01	-0.02	0.01
PD-IND			0.02		0.02 ± 0.01	-0.02	0.00
PD-BASE	AUSP	0.03	0.04	0.08	0.04 ± 0.01	-0.01	0.00
PD-RESI			0.04		0.04 ± 0.01	-0.01	0.00
PD-BIOF			0.05		0.05 ± 0.01	-0.01	0.00
PD-IND			0.04		0.04 ± 0.01	-0.01	-0.05
PD-BASE	BB	0.06	0.05	0.07	0.04 ± 0.01	0.01	0.00
PD-RESI			0.05		0.04 ± 0.01	0.01	0.00
PD-BIOF			0.06		0.05 ± 0.01	0.00	0.00
PD-IND			0.05		0.05 ± 0.01	0.00	0.00
PD-BASE	CPAO	0.03	0.04	0.06	0.04 ± 0.03	-0.01	0.00
PD-RESI			0.04		0.04 ± 0.03	-0.01	0.00
PD-BIOF			0.04		0.04 ± 0.03	-0.01	0.00
PD-IND			0.04		0.04 ± 0.03	-0.01	0.00
PD-BASE	ENPAC	0.07	0.06	0.08	0.07 ± 0.02	0.01	0.00
PD-RESI			0.06		0.07 ± 0.02	0.01	0.00
PD-BIOF			0.06		0.07 ± 0.02	0.01	0.00
PD-IND			0.06		0.07 ± 0.02	0.02	0.17
PD-BASE	NATL	0.05	0.07	0.12	0.07 ± 0.02	-0.02	0.00
PD-RESI			0.07		0.07 ± 0.02	-0.02	0.00
PD-BIOF			0.07		0.07 ± 0.02	-0.02	0.00
PD-IND			0.06		0.06 ± 0.01	-0.01	0.00
PD-BASE	SATL	0.02	0.03	0.04	0.03 ± 0.01	-0.01	0.00
PD-RESI			0.03		0.03 ± 0.01	-0.01	0.00
PD-BIOF			0.04		0.03 ± 0.01	-0.01	-0.21
PD-IND			0.03		0.03 ± 0.01	-0.01	0.00
PD-BASE	SEAS	0.07	0.04	0.07	0.06 ± 0.04	0.02	0.00
PD-RESI			0.04		0.06 ± 0.04	0.02	0.00
PD-BIOF			0.05		0.07 ± 0.05	0.02	0.02
PD-IND			0.05		0.06 ± 0.04	0.02	0.19
PD-BASE	SO	0.05	0.03	0.13	0.03 ± 0.01	0.01	0.00
PD-RESI			0.03		0.03 ± 0.01	0.01	0.00
PD-BIOF			0.03		0.03 ± 0.01	0.01	0.16

PD-IND			0.03		0.03 ± 0.01	0.01	0.16
PD-BASE	WNPAC	0.09	0.07	0.09	0.08 ± 0.03	0.02	0.00
PD-RESI			0.07		0.08 ± 0.03	0.02	0.00
PD-BIOF			0.07		0.08 ± 0.03	0.01	0.00
PD-IND			0.06		0.07 ± 0.02	0.02	0.00

206

207

208

209

References:

Agrawal, H., Malloy, Q. G. J., Welch, W. A., Wayne Miller, J., and Cocker, D. R.: In-use gaseous and particulate matter emissions from a modern ocean going container vessel, Atmospheric Environment, 42, 5504-5510, https://doi.org/10.1016/j.atmosenv.2008.02.053, 2008.

Al-Negheimish, A. I., Al-Mutlaq, F. M., Fares, G., Alhozaimy, A. M., and Iqbal Khan, M.: Characterization of chemical accelerators for sustainable recycling of fresh electric-arc furnace dust in cement pastes, Advanced Powder Technology, 32, 3046-3062, https://doi.org/10.1016/j.apt.2021.06.019, 2021.

Alizadeh, M., and Momeni, M.: The effect of the scrap/DRI ratio on the specification of the EAF dust and its influence on mechanical properties of the concrete treated by its dust, Construction and Building Materials, 112, 1041-1045, https://doi.org/10.1016/j.conbuildmat.2016.03.011, 2016.

Alsheyab, M. A. T., and Khedaywi, T. S.: Analysis of the Effect of Temperature on the Resilient Modulus of Asphalt Concrete Mixed with Electric Arc Furnace Dust (EAFD), Water, Air, & Soil Pollution, 227, 80, 10.1007/s11270-016-2776-4, 2016.

Alves, C., Gonçalves, C., Fernandes, A. P., Tarelho, L., and Pio, C.: Fireplace and woodstove fine particle emissions from combustion of western Mediterranean wood types, Atmospheric Research, 101, 692-700, https://doi.org/10.1016/j.atmosres.2011.04.015, 2011.

Baldo, C., Ito, A., Krom, M. D., Li, W., Jones, T., Drake, N., Ignatyev, K., Davidson, N., and Shi, Z.: Iron from coal combustion particles dissolves much faster than mineral dust under simulated atmospheric acid conditions, Atmos. Chem. Phys. Discuss., 2021, 1-31, 2021.

Bayuseno, A. P., and Schmahl, W. W.: Characterization of MSWI fly ash through mineralogy and water extraction, Resources, Conservation and Recycling, 55, 524-534, 2011.

Bond, T. C., Streets, D. G., Yarber, K. F., Nelson, S. M., Woo, J.-H., and Klimont, Z.: A technology-based global inventory of black and organic carbon emissions from combustion, Journal of Geophysical Research: Atmospheres, 109, https://doi.org/10.1029/2003JD003697, 2004.

Celo, V., Dabek-Zlotorzynska, E., and McCurdy, M.: Chemical Characterization of Exhaust Emissions from Selected Canadian Marine Vessels: The Case of Trace Metals and Lanthanoids, Environmental Science & Technology, 49, 5220-5226, 10.1021/acs.est.5b00127, 2015.

Cobo, M., Gálvez, A., Conesa, J. A., and Montes de Correa, C.: Characterization of fly ash from a hazardous waste incinerator in Medellin, Colombia, Journal of hazardous materials, 168, 1223-1232, 2009.

Desboeufs, K., Sofikitis, A., Losno, R., Colin, J., and Ausset, P.: Dissolution and solubility of trace metals from natural and anthropogenic aerosol particulate matter, Chemosphere, 58, 195-203, 2005.

Dutta, B. K., Khanra, S., and Mallick, D.: Leaching of elements from coal fly ash: Assessment of its potential for use in filling abandoned coal mines, Fuel, 88, 1314-1323, 2009.

Fu, H., Lin, J., Shang, G., Dong, W., Grassian, V. H., Carmichael, G. R., Li, Y., and Chen, J.: Solubility of Iron from Combustion Source Particles in Acidic Media Linked to Iron Speciation, Environmental Science & Technology, 46, 11119-11127, 2012.

Funari, V., Mäkinen, J., Salminen, J., Braga, R., Dinelli, E., and Revitzer, H.: Metal removal from Municipal Solid Waste Incineration fly ash: A comparison between chemical leaching and bioleaching, Waste Management, 60, 397-406, 2017.

Goodarzi, F.: Characteristics and composition of fly ash from Canadian coal-fired power plants, Fuel, 85, 1418-1427, https://doi.org/10.1016/j.fuel.2005.11.022, 2006.

Hagni, A. M., Hagni, R. D., and Demars, C.: Mineralogical characteristics of electric arc furnace dusts, JOM, 43, 28-30, 10.1007/BF03220543, 1991.

Hedberg, E., Kristensson, A., Ohlsson, M., Johansson, C., Johansson, P.-Å., Swietlicki, E., Vesely, V., Wideqvist, U., and Westerholm, R.: Chemical and physical characterization of emissions from birch wood combustion in a wood stove, Atmospheric Environment, 36, 4823-4837, https://doi.org/10.1016/S1352-2310(02)00417-X, 2002.

Hildemann, L. M., Markowski, G. R., Jones, M. C., and Cass, G. R.: Submicrometer Aerosol Mass Distributions of Emissions from Boilers, Fireplaces, Automobiles, Diesel Trucks, and Meat-Cooking Operations, Aerosol Science and Technology, 14, 138-152, 10.1080/02786829108959478, 1991.

Hleis, D., Fernández-Olmo, I., Ledoux, F., Kfoury, A., Courcot, L., Desmonts, T., and Courcot, D.: Chemical profile identification of fugitive and confined particle emissions from an integrated iron and steelmaking plant, Journal of hazardous materials, 250-251, 246-255, https://doi.org/10.1016/j.jhazmat.2013.01.080, 2013.

Hoesly, R. M., Smith, S. J., Feng, L., Klimont, Z., Janssens-Maenhout, G., Pitkanen, T., Seibert, J. J., Vu, L., Andres, R. J., Bolt, R. M., Bond, T. C., Dawidowski, L., Kholod, N., Kurokawa, J. I., Li, M., Liu, L., Lu, Z., Moura, M. C. P., O'Rourke, P. R., and Zhang, Q.: Historical (1750–2014) anthropogenic emissions of reactive gases and aerosols from the Community Emissions Data System (CEDS), Geoscientific Model Development, 11, 369-408, 10.5194/gmd-11-369-2018, 2018.

Jankowski, J., Ward, C. R., French, D., and Groves, S.: Mobility of trace elements from selected Australian fly ashes and its potential impact on aquatic ecosystems, Fuel, 85, 243-256, 2006.

Laforest, G., and Duchesne, J.: Stabilization of electric arc furnace dust by the use of cementitious materials: Ionic competition and long-term leachability, Cement and Concrete Research, 36, 1628-1634, https://doi.org/10.1016/j.cemconres.2006.05.012, 2006.

Li, C., Liu, W., Jiao, F., Yang, C., Li, G., Liu, S., and Qin, W.: Separation and recovery of zinc, lead and iron from electric arc furnace dust by low temperature smelting, Separation and Purification Technology, 312, 123355, https://doi.org/10.1016/j.seppur.2023.123355, 2023.

Li, R., Zhang, H., Wang, F., He, Y., Huang, C., Luo, L., Dong, S., Jia, X., and Tang, M.: Mass fractions, solubility, speciation and isotopic compositions of iron in coal and municipal waste fly ash, Science of The Total Environment, 838, 155974, https://doi.org/10.1016/j.scitotenv.2022.155974, 2022.

Li, S., Zhang, B., Wu, D., Li, Z., Chu, S.-Q., Ding, X., Tang, X., Chen, J., and Li, Q.: Magnetic Particles Unintentionally Emitted from Anthropogenic Sources: Iron and Steel Plants, Environmental Science & Technology Letters, 8, 295-300, 10.1021/acs.estlett.1c00164, 2021.

Lin, K. L., Wang, K. S., Tzeng, B. Y., and Lin, C. Y.: The reuse of municipal solid waste incinerator fly ash slag as a cement substitute, Resources, Conservation and Recycling, 39, 315-324, 2003.

Liu, Y., Zheng, L., Li, X., and Xie, S.: SEM/EDS and XRD characterization of raw and washed MSWI fly ash sintered at different temperatures, Journal of hazardous materials, 162, 161-173, 2009.

Loaiza, A., Cifuentes, S., and Colorado, H. A.: Asphalt modified with superfine electric arc furnace steel dust (EAF dust) with high zinc oxide content, Construction and Building Materials, 145, 538-547, https://doi.org/10.1016/j.conbuildmat.2017.04.050, 2017.

Machado, J. G. M. S., Brehm, F. A., Moraes, C. A. M., Santos, C. A. d., Vilela, A. C. F., and Cunha, J. B. M. d.: Chemical, physical, structural and morphological characterization of the electric arc furnace dust, Journal of hazardous materials, 136, 953-960, https://doi.org/10.1016/j.jhazmat.2006.01.044, 2006.

Meij, R.: Trace element behavior in coal-fired power plants, Fuel Processing Technology, 39, 199-217, https://doi.org/10.1016/0378-3820(94)90180-5, 1994.

Moreno, N., Querol, X., Andrés, J. M., Stanton, K., Towler, M., Nugteren, H., Janssen-Jurkovicová, M., and Jones, R.: Physico-chemical characteristics of European pulverized coal combustion fly ashes, Fuel, 84, 1351-1363, 2005.

Oakes, M., Ingall, E. D., Lai, B., Shafer, M. M., Hays, M. D., Liu, Z. G., Russell, A. G., and Weber, R. J.: Iron Solubility Related to Particle Sulfur Content in Source Emission and Ambient Fine Particles, Environmental Science & Technology, 46, 6637-6644, 2012.

Patil, R. S., Kumar, R., Menon, R., Shah, M. K., and Sethi, V.: Development of particulate matter speciation profiles for major sources in six cities in India, Atmospheric Research, 132-133, 1-11, https://doi.org/10.1016/j.atmosres.2013.04.012, 2013.

Raclavská, H., Corsaro, A., Hartmann-Koval, S., and Juchelková, D.: Enrichment and distribution of 24 elements within the sub-sieve particle size distribution ranges of fly ash from wastes incinerator plants, Journal of Environmental Management, 203, 1169-1177, 2017.

Rathod, S. D., Hamilton, D. S., Mahowald, N. M., Klimont, Z., Corbett, J. J., and Bond, T. C.: A Mineralogy-Based Anthropogenic Combustion-Iron Emission Inventory, Journal of Geophysical Research: Atmospheres, 125, e2019JD032114, https://doi.org/10.1029/2019JD032114, 2020.

Schmidl, C., Marr, I. L., Caseiro, A., Kotianová, P., Berner, A., Bauer, H., Kasper-Giebl, A., and Puxbaum, H.: Chemical characterisation of fine particle emissions from wood stove combustion of common woods growing in mid-European Alpine regions, Atmospheric Environment, 42, 126-141, https://doi.org/10.1016/j.atmosenv.2007.09.028, 2008.

Schroth, A. W., Crusius, J., Sholkovitz, E. R., and Bostick, B. C.: Iron solubility driven by speciation in dust sources to the ocean, Nature Geoscience, 2, 337-340, 2009.

Silva, V. S., Silva, J. S., Costa, B. d. S., Labes, C., and Oliveira, R. M. P. B.: Preparation of glaze using electric-arc furnace dust as raw material, Journal of Materials Research and Technology, 8, 5504-5514, https://doi.org/10.1016/j.jmrt.2019.09.018, 2019.

Sippula, O., Hokkinen, J., Puustinen, H., Yli-Pirilä, P., and Jokiniemi, J.: Comparison of particle emissions from small heavy fuel oil and wood-fired boilers, Atmospheric Environment, 43, 4855-4864, https://doi.org/10.1016/j.atmosenv.2009.07.022, 2009.

Sippula, O., Stengel, B., Sklorz, M., Streibel, T., Rabe, R., Orasche, J., Lintelmann, J., Michalke, B., Abbaszade, G., Radischat, C., Gröger, T., Schnelle-Kreis, J., Harndorf, H., and Zimmermann, R.: Particle Emissions from a Marine Engine: Chemical Composition and Aromatic Emission Profiles under Various Operating Conditions, Environmental Science & Technology, 48, 11721-11729, 10.1021/es502484z, 2014.

Souza, C. A. C. D., Machado, A. T., Lima, L. R. P. d. A., and Cardoso, R. J. C.: Stabilization of electric-arc furnace dust in concrete, Materials Research, 13, 513-519, 2010.

Stathopoulos, V. N., Papandreou, A., Kanellopoulou, D., and Stournaras, C. J.: Structural ceramics containing electric arc furnace dust, Journal of hazardous materials, 262, 91-99, https://doi.org/10.1016/j.jhazmat.2013.08.028, 2013.

Vieira, C. M. F., Sanchez, R., Monteiro, S. N., Lalla, N., and Quaranta, N.: Recycling of electric arc furnace dust into red ceramic, Journal of Materials Research and Technology, 2, 88-92, https://doi.org/10.1016/j.jmrt.2012.09.001, 2013.

Wan, X., Wang, W., Ye, T., Guo, Y., and Gao, X.: A study on the chemical and mineralogical characterization of

MSWI fly ash using a sequential extraction procedure, Journal of hazardous materials, 134, 197-201, 2006.

Watson, J. G., Chow, J. C., and Houck, J. E.: PM2.5 chemical source profiles for vehicle exhaust, vegetative burning, geological material, and coal burning in Northwestern Colorado during 1995, Chemosphere, 43, 1141-1151, https://doi.org/10.1016/S0045-6535(00)00171-5, 2001.

Wu, H.-Y., and Ting, Y.-P.: Metal extraction from municipal solid waste (MSW) incinerator fly ash—Chemical leaching and fungal bioleaching, Enzyme and Microbial Technology, 38, 839-847, 2006.

Wu, K., Shi, H., Schutter, G. D., Guo, X., and Ye, G.: Preparation of alinite cement from municipal solid waste incineration fly ash, Cement and Concrete Composites, 34, 322-327, 2012.

Xia, D. K., and Picklesi, C. A.: Microwave caustic leaching of electric arc furnace dust, Minerals Engineering, 13, 79-94, https://doi.org/10.1016/S0892-6875(99)00151-X, 2000.

Ye, L., Peng, Z., Ye, Q., Wang, L., Augustine, R., Perez, M., Liu, Y., Liu, M., Tang, H., Rao, M., Li, G., and Jiang, T.: Toward environmentally friendly direct reduced iron production: A novel route of comprehensive utilization of blast furnace dust and electric arc furnace dust, Waste Management, 135, 389-396, https://doi.org/10.1016/j.wasman.2021.08.045, 2021.

Zhang, H., Li, R., Dong, S., Wang, F., Zhu, Y., Meng, H., Huang, C., Ren, Y., Wang, X., Hu, X., Li, T., Peng, C., Zhang, G., Xue, L., Wang, X., and Tang, M.: Abundance and Fractional Solubility of Aerosol Iron During Winter at a Coastal City in Northern China: Similarities and Contrasts Between Fine and Coarse Particles, Journal of Geophysical Research: Atmospheres, 127, e2021JD036070, https://doi.org/10.1029/2021JD036070, 2022.

Zhang, H., Zhao, Y., and Qi, J.: Utilization of municipal solid waste incineration (MSWI) fly ash in ceramic brick: Product characterization and environmental toxicity, Waste Management, 31, 331-341, 2011.

Zhang, H., Wang, S., Hao, J., Wan, L., Jiang, J., Zhang, M., Mestl, H. E. S., Alnes, L. W. H., Aunan, K., and Mellouki, A. W.: Chemical and size characterization of particles emitted from the burning of coal and wood in rural households in Guizhou, China, Atmospheric Environment, 51, 94-99, https://doi.org/10.1016/j.atmosenv.2012.01.042, 2012.